Supplementary Material for

Periodically-arrayed ferroelectric nanostructures induced by dislocation structures in strontium titanate

Kairi MASUDA[*1], Le Van Lich[*2], Takahiro SHIMADA[*1] and Takayuki KITAMURA[*1]
[*1] Department of Mechanical Engineering and Science, Kyoto University
Kyoto-daigaku-katsura, Nishikyo-ku, Kyoto 615-8540, Japan
[*2] School of Materials Science and Engineering, Hanoi University of Science and Technology
No 1, Dai Co Viet Street, Hanoi, Viet Nam

1 Phase-Field modeling of $SrTiO_3$

1.1 Interactions of strain, polarization, and AFD in $SrTiO_3$

Figure S1 shows the crystal structure of $SrTiO_3$. Under the stress-free condition, the crystal structure is the perfect cubic structure as shown in Fig. S1(a). This cubic structure is called the paraelectric (PE) phase, and $SrTiO_3$ does not exhibit any spontaneous polarization. On the other hand, $SrTiO_3$ subject to tensile strain above a certain intensity exhibits spontaneous polarization along the tensile direction (Fig. S1(b))[1–3]. This structure is the ferroelectric (FE) phase with displacements of cations (Sr^{2+}, Ti^{4+}) and anions (O^{2-}) from the ideal lattice positions. Thus, $SrTiO_3$ transforms from PE to FE by mechanical loading. Furthermore, at low temperature, $SrTiO_3$ exhibits the antiferrodistortive (AFD) phase, in which the oxygen octahedral rotates as shown in Fig. S1(c)[4]. The AFD and FE compete with each other[5]. Thus, strain, polarization, and AFD are coupled with each other in $SrTiO_3$. To construct phase-field modeling of $SrTiO_3$, these interactions must be incorporated into free energy.

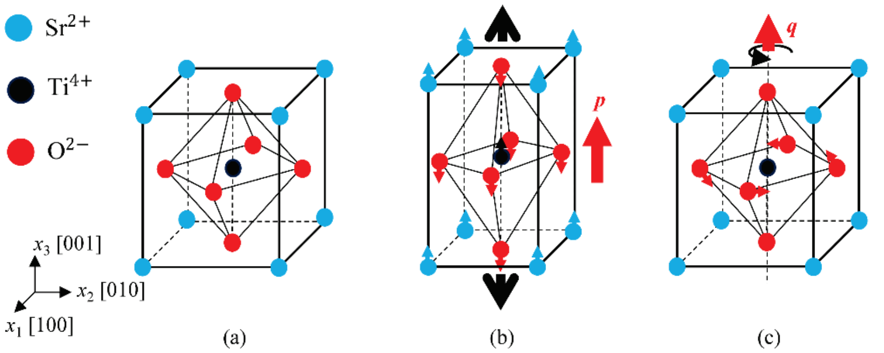

Figure S1. Crystal structures of $SrTiO_3$ (a) in the paraelectric phase, (b) in the ferroelectric phase under uniaxial strain along [001] and (c) in the AFD phase.

1.2 Free energy of SrTiO$_3$

Taking polarization $\boldsymbol{p} = (p_1, p_2, p_3)$ and AFD $\boldsymbol{q} = (q_1, q_2, q_3)$ as the order parameters, the total free energy F can be shown as[6–8]

$$F = \int_V f dv = \int_V (f_{bulk} + f_{elas} + f_{grad} + f_{elec}) dv, \tag{S1}$$

where f, f_{bulk}, f_{elas}, f_{grad}, and f_{elec} denote the total free energy density, the Landau energy density, the elastic energy density, the gradient free energy density, and the electrostatic energy density. V denotes the entire volume of the SrTiO$_3$ system.

The Landau energy density f_{bulk} is expressed as

$$\begin{aligned} f_{bulk} = {} & \alpha_1(p_1^2 + p_2^2 + p_3^2) + \alpha_{11}(p_1^4 + p_2^4 + p_3^4) + \alpha_{12}(p_1^2 p_2^2 + p_2^2 p_3^2 + p_3^2 p_1^2) \\ & + \beta_1(q_1^2 + q_2^2 + q_3^2) + \beta_{11}(q_1^4 + q_2^4 + q_3^4) + \beta_{12}(q_1^2 q_2^2 + q_2^2 q_3^2 + q_3^2 q_1^2) \\ & - t_{11}(p_1^2 q_1^2 + p_2^2 q_2^2 + p_3^2 q_3^2) \\ & - t_{12}(p_1^2(q_2^2 + q_3^2) + p_2^2(q_3^2 + q_1^2) + p_3^2(q_1^2 + q_2^2)) \\ & - t_{44}(p_1 p_2 q_1 q_2 + p_2 p_3 q_2 q_3 + p_3 p_1 q_3 q_1), \end{aligned} \tag{S2}$$

where α_1, α_{ij}, β_1, β_{ij} and t_{ij} are the Landau coefficients related to polarization, AFD and the coupling of polarization and AFD. The Landau energy density represents the property of polarization and AFD. Especially, the seventh, eighth and ninth term exhibit the coupling between polarization and AFD. The interaction of polarization and AFD is represented by these terms.

The elastic energy density is given by

$$f_{elas} = \frac{1}{2} c_{ijkl} e_{ij} e_{kl} = \frac{1}{2} c_{ijkl} (\varepsilon_{ij} - \varepsilon_{ij}^0)(\varepsilon_{kl} - \varepsilon_{kl}^0), \tag{S3}$$

where c_{ijkl} denotes the elastic stiffness tensor. e_{ij} and ε_{ij} are elastic strain and total strain, respectively. ε_{ij}^0 is eigen-strain induced by polarization and AFD shown as

$$\varepsilon_{ij}^0 = Q_{ijkl} p_k p_l + \Lambda_{ijkl} q_k q_l, \tag{S4}$$

where Q_{ijkl} and Λ_{ijkl} represent the electrostrictive coefficients and the coupling coefficients between strain and AFD, respectively. The expanded elastic energy density is given by

$$
\begin{aligned}
f_{clas} &= \frac{1}{2}c_{11}\left(\varepsilon_{11}^2+\varepsilon_{22}^2+\varepsilon_{33}^2\right)+c_{12}\left(\varepsilon_{11}\varepsilon_{22}+\varepsilon_{22}\varepsilon_{33}+\varepsilon_{33}\varepsilon_{11}\right)+2c_{44}\left(\varepsilon_{12}^2+\varepsilon_{23}^2+\varepsilon_{33}^2\right) \\
&-\left(c_{11}Q_{11}+2c_{12}Q_{12}\right)\left(\varepsilon_{11}p_1^2+\varepsilon_{22}p_2^2+\varepsilon_{33}p_3^2\right) \\
&-\left\{c_{11}Q_{12}+c_{12}\left(Q_{11}+Q_{12}\right)\right\}\left\{\varepsilon_{11}\left(p_2^2+p_3^2\right)+\varepsilon_{22}\left(p_1^2+p_3^2\right)+\varepsilon_{33}\left(p_1^2+p_2^2\right)\right\} \\
&-2c_{44}Q_{44}\left(\varepsilon_{12}p_1p_2+\varepsilon_{23}p_2p_3+\varepsilon_{13}p_1p_3\right) \\
&-\left(c_{11}\Lambda_{11}+2c_{12}\Lambda_{12}\right)\left(\varepsilon_{11}q_1^2+\varepsilon_{22}q_2^2+\varepsilon_{33}q_3^2\right) \\
&-\left\{c_{11}\Lambda_{12}+c_{12}\left(\Lambda_{11}+\Lambda_{12}\right)\right\}\left\{\varepsilon_{11}\left(q_2^2+q_3^2\right)+\varepsilon_{22}\left(q_1^2+q_3^2\right)+\varepsilon_{33}\left(q_1^2+q_2^2\right)\right\} \\
&-2c_{44}\Lambda_{44}\left(\varepsilon_{12}q_1q_2+\varepsilon_{23}q_2q_3+\varepsilon_{13}q_1q_3\right) \\
&+\frac{1}{2}\left\{c_{11}\left(Q_{11}^2+2Q_{12}^2\right)+2c_{12}Q_{12}\left(2Q_{11}+Q_{12}\right)\right\}\left(p_1^4+p_2^4+p_3^4\right) \\
&+\left\{c_{11}Q_{12}\left(2Q_{11}+Q_{12}\right)+c_{12}\left(Q_{11}^2+3Q_{12}^2+2Q_{11}Q_{12}\right)+2c_{44}Q_{44}^2\right\}\left(p_1^2p_2^2+p_2^2p_3^2+p_3^2p_1^2\right) \\
&+\frac{1}{2}\left\{c_{11}\left(\Lambda_{11}^2+2\Lambda_{12}^2\right)+2c_{12}\Lambda_{12}\left(2\Lambda_{11}+\Lambda_{12}\right)\right\}\left(q_1^4+q_2^4+q_3^4\right) \\
&+\left\{c_{11}\Lambda_{12}\left(2\Lambda_{11}+\Lambda_{12}\right)+c_{12}\left(\Lambda_{11}^2+3\Lambda_{12}^2+2\Lambda_{11}\Lambda_{12}\right)+2c_{44}\Lambda_{44}^2\right\}\left(q_1^2q_2^2+q_2^2q_3^2+q_3^2q_1^2\right) \\
&+\left[c_{11}\left(Q_{11}\Lambda_{11}+2Q_{12}\Lambda_{12}\right)+2c_{12}\left\{Q_{11}\Lambda_{12}+Q_{12}\left(\Lambda_{11}+\Lambda_{12}\right)\right\}\right]\left(p_1^2q_1^2+p_2^2q_2^2+p_3^2q_3^2\right) \\
&+\left[c_{11}\left\{Q_{11}\Lambda_{12}+Q_{12}\left(\Lambda_{11}+\Lambda_{12}\right)\right\}+c_{12}\left\{\left(Q_{11}+Q_{12}\right)\left(\Lambda_{11}+\Lambda_{12}\right)+2Q_{12}\Lambda_{12}\right\}\right. \\
&\left.\left\{p_1^2\left(q_2^2+q_3^2\right)+p_2^2\left(q_3^2+q_1^2\right)+p_3^2\left(q_1^2+q_2^2\right)\right\}\right. \\
&+4c_{44}Q_{44}\Lambda_{44}\left(p_1p_2q_1q_2+p_2p_3q_2q_3+p_3p_1q_3q_1\right),
\end{aligned}
\tag{S5}
$$

where, following the Voigt notation, $c_{11} = c_{1111}$, $c_{12} = c_{1122}$, $c_{44} = c_{1212}$, $Q_{11} = Q_{1111}$, $Q_{12} = Q_{1122}$, $Q_{44} = Q_{1212}/2$, $\Lambda_{11} = \Lambda_{1111}$, $\Lambda_{12} = \Lambda_{1122}$ and $\Lambda_{44} = \Lambda_{1212}/2$, respectively. Especially, the fourth, fifth and sixth term exhibit the coupling between polarization and strain. The interaction of polarization and strain is represented by these terms.

The gradient energy density, which is the penalty for the spatially inhomogeneous order parameters, is described as

$$
\begin{aligned}
f_{glad} &= \frac{1}{2}G_p(p_{1,1}^2+p_{1,2}^2+p_{1,3}^2+p_{2,1}^2+p_{2,2}^2+p_{2,3}^2+p_{3,1}^2+p_{3,2}^2+p_{3,3}^2) \\
&+\frac{1}{2}G_q(q_{1,1}^2+q_{1,2}^2+q_{1,3}^2+q_{2,1}^2+q_{2,2}^2+q_{2,3}^2+q_{3,1}^2+q_{3,2}^2+q_{3,3}^2),
\end{aligned}
\tag{S6}
$$

where G_p and G_q are the gradient coefficients related to polarization and AFD, respectively. $p_{i,j} = \delta p_i/\delta x_j$ and $q_{i,j} = \delta p_i/\delta x_j$ are gradients of polarization and AFD using the position vector $\boldsymbol{x} = (x_1, x_2, x_3)$.

The electrostatic energy density is given as

$$f_{elec} = -\frac{1}{2}\varepsilon_0(\kappa_{11}E_1^2 + \kappa_{22}E_2^2 + \kappa_{33}E_3^2) - (E_1p_1 + E_2p_2 + E_3p_3), \tag{S7}$$

where E_i and ε_0 denote electric field components and the permittivity of vacuum. κ_{ij} is the relative dielectric permittivity of $SrTiO_3$.

The total free energy mentioned above includes the interactions of strain, polarization, and AFD, which are essential to describe the properties of $SrTiO_3$.

1.3 Governing equations in $SrTiO_3$

The temporal and spatial evolution of polarization and AFD are calculated by the time-dependent Ginzburg-Landau (TDGL) equations,

$$\frac{\partial p_i(\mathbf{x},t)}{\partial t} = -L_p\frac{\delta F}{\delta p_i(\mathbf{x},t)}, \tag{S8}$$

$$\frac{\partial q_i(\mathbf{x},t)}{\partial t} = -L_q\frac{\delta F}{\delta q_i(\mathbf{x},t)}, \tag{S9}$$

where t represents time. L_p and L_q are the kinetic coefficients related to the domain mobility for polarization and AFD, respectively. $\delta F/\delta p_{\mathrm{i}}$ and $\delta F/\delta q_{\mathrm{i}}$ denote the thermodynamic driving forces for polarization and AFD evolutions. In addition to the time-dependent Ginzburg-Landau equations, the following mechanical equilibrium equation

$$\frac{\partial}{\partial x_j}\left(\frac{\partial f}{\partial \varepsilon_{ij}}\right) = 0, \tag{S10}$$

and Maxwell-Gauss equation

$$\frac{\partial}{\partial x_i}\left(-\frac{\partial f}{\partial E_i}\right) = 0, \tag{S11}$$

must be satisfied for charge and body force free ferroelectric materials simultaneously.

2 Simulation models

2.1 Simulation model of an isolated edge dislocation

Figure S2(a) shows the simulation model of an edge dislocation in a bulk $SrTiO_3$. The model consists of a single crystal of $SrTiO_3$ in which the crystal orientation [100], [010], and [001] corresponds to the x_1, x_2, and x_3 axis of the model. The size of the simulation model in the x_1 and x_2 directions is 128 nm×128 nm, using 256×256 grids whose grid spacing is 0.5 nm. In a discretized system, the eigen-strain of an [100](010) edge dislocation at grid (x_0, y_0) is described as [9,10]

$$\varepsilon_{11}^{d,eigen}(\mathbf{r}) = -\frac{b}{d_0}\delta(x-x_0)H(y-y_0), \tag{S12}$$

where b and d_0 are the magnitudes of the Burgers vector and the grid spacing. $\delta(x)$ is the Dirac delta function and $H(y)$ is the Heaviside step function, respectively. In this study, the eigen-strain corresponded with an edge dislocation is set at the center of the simulation model, i.e., (x_0, y_0) = (128,128). The periodic boundary conditions are applied to the simulation cell in the x_1, x_2 and x_3 directions to realize an isolated dislocation in the bulk $SrTiO_3$. The values of the material coefficients are given in Table S1[6,11].

2.2 Simulation model of dislocation dipoles

Figure S2(b1) shows the simulation model of a dislocation dipole (the dipole A). Same as the simulation model for an isolated edge dislocation, the model consists of 128 nm×128 nm single crystal $SrTiO_3$. The eigen-strain corresponded with the dislocation dipole, i.e., [±100](010) is set at the center of the model. The spacing and the angle between dislocations are 14 nm and 45 degrees, respectively. The periodic boundary conditions are applied to the simulation cell in the x_1, x_2 and x_3 directions to realize the dislocation dipole in the bulk $SrTiO_3$. The values of the material coefficients for $SrTiO_3$ are the same as those for an isolated edge dislocation. In addition, to investigate the effect of dislocation arrangements on the ferroelectricity, we study the dipole B shown in Fig. S2(b2) in the same manner as the dipole A.

2.3 Simulation model of a dislocation wall

Figure S2(c) shows the simulation model of a dislocation wall. Same as the simulation model for an isolated edge dislocation, the model consists of a single crystal of $SrTiO_3$ in which the crystal orientation [100], [010] and [001] corresponds to the x_1, x_2 and x_3 axis of the model. The size of the simulation model in the x_1 and x_2 directions is 180 nm×180 nm, using 360×360 grids whose grid spacing is 0.5 nm. The eigen-strain corresponded to nine dislocation dipoles is set in the x_2 direction. The periodic boundary conditions are applied to the simulation cell in the x_1, x_2, and x_3 directions to realize the dislocation wall in the bulk $SrTiO_3$. The values of the material coefficients for $SrTiO_3$ are same as those for an isolated edge dislocation.

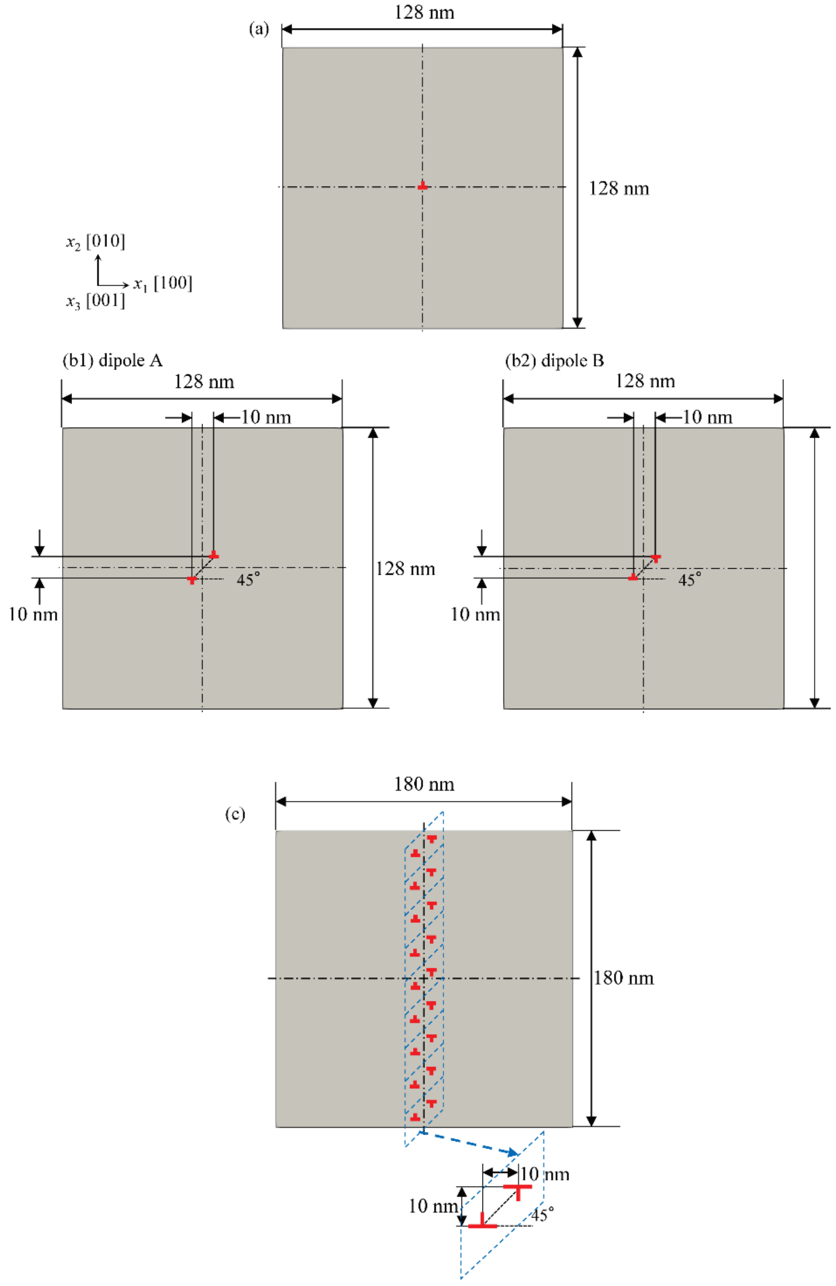

Figure S2 Simulation models of dislocation structures in a bulk $SrTiO_3$ and its dimensions. Dislocation marks indicate where dislocations are set. (a) an isolated edge dislocation. (b) Dislocation dipoles. (c) Dislocation wall. The distance between dislocatins is $10\sqrt{2} \approx 14$ nm.

Table S1 Material constants for $SrTiO_3$ used in the simulation

Landau coefficient for polarization		Landau coefficient for AFD	
α_1 [dyn cm^2/stac^2]	4.5×10^{-3}[coth(54/T)−coth(54/30)]	β_1 [dyn/cm^4]	1.32×10^{26}[coth(145/T)−coth(145/105)]
α_{11} [dyn cm^6/stac^4]	2.1×10^{-12}	β_{11} [dyn/cm^6]	1.69×10^{43}
α_{12} [dyn cm^6/stac^4]	4.85×10^{-12}	β_{12} [dyn/cm^6]	3.88×10^{43}
Coupling coefficient for polarization		Coupling coefficient for AFD	
Q_{11} [cm^4/stac^2]	5.09×10^{-13}	Λ_{11} [/cm^2]	8.7×10^{14}
Q_{12} [cm^4/stac^2]	-1.50×10^{-13}	Λ_{12} [/cm^2]	-7.8×10^{14}
Q_{44} [cm^4/stac^2]	1.065×10^{-13}	Λ_{44} [/cm^2]	-9.2×10^{14}
Elastic constants		Relative gradient constants	
c_{11} [dyn/cm^2]	3.36×10^{12}	G_p/G_0	0.4
c_{12} [dyn/cm^2]	1.07×10^{12}	G_q/G_p	0.012
c_{44} [dyn/cm^2]	1.27×10^{12}	Relative dielectric constant	
		κ	300
		Burgers vector for [100](010)	
		b [nm]	0.39

3 Simulation procedures

3.1 Calculation of strain fields around dislocations

At first, we numerically calculate the elastic fields induced by an edge dislocation from the eigen-strain. In the numerical simulation, it is difficult to directly use discontinuous functions such as eigen-strain of dislocations. To overcome this problem, it is proposed to smooth discontinuous functions by convolution integral with Gauss functions. The eigen-strain smoothed by Gauss functions is shown as[9]

$$\varepsilon_{11}^{d,eigen}(\mathbf{r}) = -\frac{b}{d_0}\iint e^{-\left\{(x-x_0)^2+(y-y_0)^2\right\}}\delta(x-x_1)H(y-y_1)dx_1dy_1. \tag{S13}$$

The corresponding Fourier transformation is given by

$$\tilde{\varepsilon}_{11}^{d,eigen}(\mathbf{q}) = -\frac{b}{d_0}\frac{I}{q_2V}e^{I(q_1x_0+q_2y_0)}e^{-\left(\frac{q_1^2}{4}+\frac{q_2^2}{4}\right)}, \tag{S14}$$

where I is an imaginary number, $\mathbf{q}$ is a unit vector in the reciprocal space, and V is the volume of the model. From this smoothed eigen-strain, the elastic fields in the Fourier space are calculated numerically by

$$\tilde{\varepsilon}_{mn}^{d,elas}(\mathbf{q}) = \frac{I}{2}[v_i(\mathbf{q})q_j + v_j(\mathbf{q})q_i] - \tilde{\varepsilon}_{mn}^{d,eigen}(\mathbf{q}), \tag{S15}$$

$$v_i(\mathbf{q}) = -IG_{ik}(\mathbf{q})q_jc_{ijmn}\tilde{\varepsilon}_{mn}^{d,eigen}(\mathbf{q}), \tag{S16}$$

where $G_{im}(\mathbf{q})$, $\tilde{\varepsilon}_{mn}^{d,elas}(\mathbf{q})$ and $\tilde{\varepsilon}_{kl}^{d,eigen}(\mathbf{q})$ are the Green tensor whose inverse tensor is defined as $G_{im}^{-1}(\mathbf{q}) = c_{ijml}q_jq_l$ and the Fourier transforms of $\varepsilon_{mn}^{d,elas}(\mathbf{r})$ and $\varepsilon_{kl}^{d,eigen}(\mathbf{r})$, respectively. By the inverse Fourier transformation, the dislocation-induced elastic field in the real space $\varepsilon_{ij}^{d,elas}(\mathbf{r})$ is obtained.

To validate the numerical solution, we compare it with the analytical solution. The analytical solution of an edge dislocation is given as[12]

$$\varepsilon_{11}^{analytical}(\mathbf{x}) = -\frac{b}{2\pi}\frac{\{(2\lambda+3\mu)x_1^2+\mu x_2^2\}}{(2\lambda+3\mu)(x_1^2+x_2^2)^2}, \tag{S17}$$

where λ and μ are the Lame parameters. We employ $\lambda = c_{12}$ and $\mu = c_{44}$ assuming that $SrTiO_3$ is an isotropic elastic medium. Figure S3 shows strain distributions obtained from the numerical and the analytical solution. The strain distribution from the numerical solution (Fig. S3(a1)) is in good agreement with that from the analytical solution (Fig. S3(a2)). Therefore, the qualitative property of a dislocation, i.e., the shape of strain distribution is obtained from the numerical solution. Figure S3(b) shows the profile of the elastic strain field. The strain from the numerical solution is in good agreement with that from the analytical solution quantitatively. Therefore, the strain field of dislocations is obtained from the numerical solution.

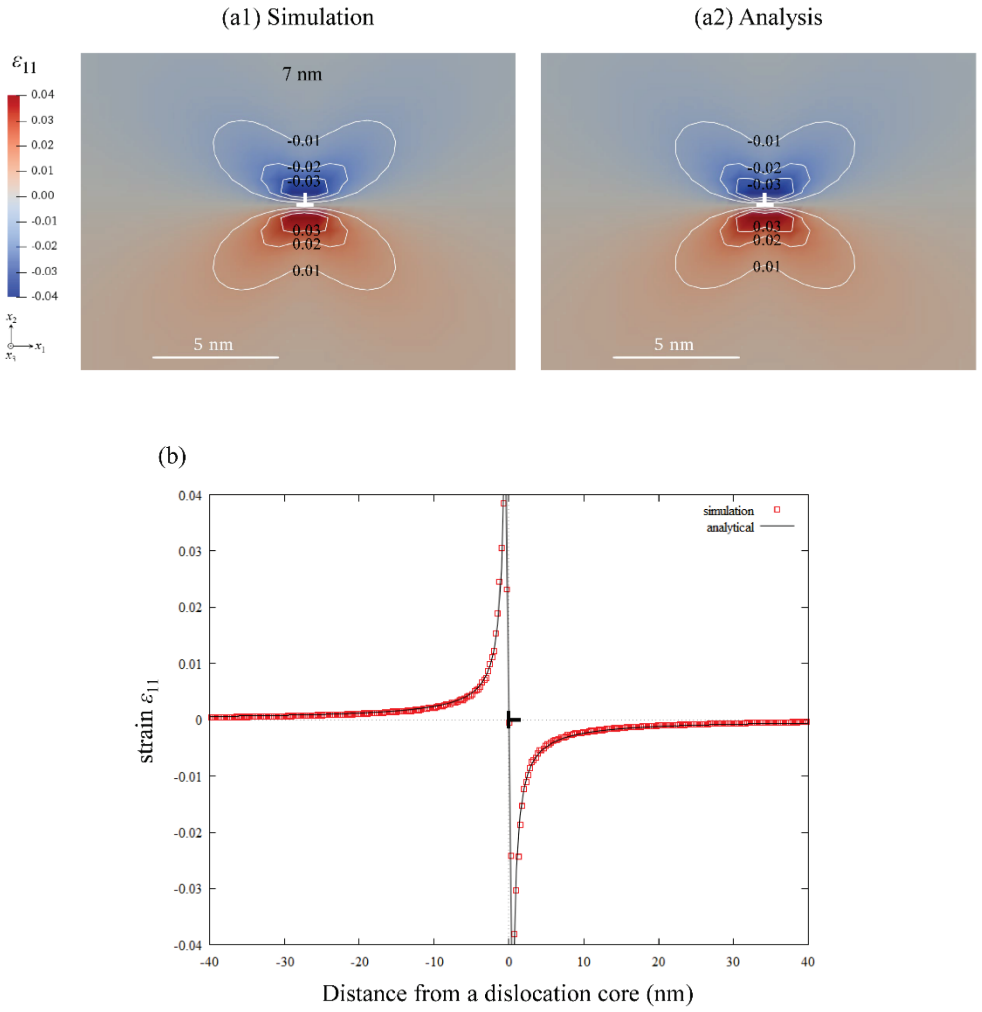

Figure S3 The elastic strain ε_{11} distribution around a dislocation core obtained from (a1) the numerical solution and (a2) analytical solution. The contour indicates the elastic strain intensity. White line indicates $|\varepsilon_{11}| = 0.01$, 0.02 and 0.03. (b) The elastic strain ε_{11} profile around a dislocation. Red open squares indicate the numerical solution and a black solid line indicates the analytical solution.

3.2 Phase field simulation

Next, we numerically calculate polarization distributions around an edge dislocation in the bulk $SrTiO_3$ by solving governing equations. Here, the simulation is conducted at room temperature (T = 300 K) and we ignore AFD which appears at low temperature (T = 105 K). The elastic strain $\varepsilon_{ij}^{elas}(\mathbf{r})$ can be divided into[13].

$$\varepsilon_{ij}^{elas}(\mathbf{r}) = \varepsilon_{ij}^{p,total}(\mathbf{r}) - \varepsilon_{ij}^{p,eigen}(\mathbf{r}) + \varepsilon_{ij}^{d,elas}(\mathbf{r}), \tag{S18}$$

where $\varepsilon_{ij}^{p,eigen}(\mathbf{r})$ is the eigen-strain of polarization and $\varepsilon_{ij}^{p,total}(\mathbf{r})$ is the total strain related to polarization. By calculating the elastic energy density incorporating $\varepsilon_{ij}^{d,elas}(\mathbf{r})$ obtained from the eigen-strain, we introduce an edge dislocation into the bulk $SrTiO_3$.

To obtain the thermodynamic equilibrium state, a random distribution of polarization with small magnitudes 1×10^{-5} C/m^2 is introduced as the initial state. The mechanical equilibrium equation and Maxwell-Gauss equation are numerically solved using the Fourier spectral iterative perturbation method[14–17]. Then, the time evolution of polarization at the normalized time step $\Delta t/t_0 = 0.05$ ($t_0 = L_p|\alpha_1|$) is calculated by numerically solving the TDGL equation using the semi-implicit Fourier-spectral method[18,19]. To determine the thermodynamic equilibrium state, the mechanical equilibrium equation, Maxwell-Gauss equation, and TDGL equation are solved repeatedly until the change of polarization at each time step becomes less than 1×10^{-5} C/m^2. Polarization distributions around the dipoles and the dislocation wall are calculated in the same manner as an edge dislocation.

4 Physical field around a dislocation wall

In this section, we consider two questions based on physical fields around the dislocation wall: (1) why ferroelectric nano-region connects in dipole B in the dislocation wall, and (2) why the connected ferroelectric nano-region between dipole B is larger than that around dipole A.

Figure S4 shows the polarization distribution, strain field, polarization magnitude, and electric field around a dislocation wall. As shown in Figs. 4(b1), (b2) in the main text, the tensile region around one dislocation expands in dipole A and shrinks in dipole B. On the other hand, in the dislocation wall, one dislocation belongs to dipole A and B at the same time. Therefore, one dislocation undergoes expanding and shrinking simultaneously. In other words, the tensile region around dipole B gets stronger by nearby dipole A (Fig. S4(b2)). As a result, in the dislocation wall, the maximum of polarization value is about 0.23 C/m^2 around dipole B (Fig. S4(c2)) while the maximum of polarization value around the isolated dipole B is about 0.19 C/m^2. Therefore, the polarization magnitude around dipole B increases in the wall.

Electric fields are induced depending on the magnitude of tensile-region-induced polarization as shown in Fig 1(d) in the main text. Therefore, in the dislocation wall, electric fields around dipole B become larger than that around the isolated dipole B (Fig. S4(d2)). As a result, since ferroelectric nano-region is also formed by electric field, ferroelectric nano-region around dipole B expands in the dislocation wall compared with the isolated dipole B. Consequently, ferroelectric nano-region connects even in dipole B in the wall. And the dipole A is contrary to dipole B, that is, since the tensile region and electric field shrinks, the connectivity of ferroelectric nano-region gets weaker (Fig. S4(b1) - (d1)).

Here, it should be noted that, in SrTiO$_3$, strain has two roles: the appearance of polarization and enhancement of polarization (piezoelectricity). In dislocation structures, although compression does not contribute to the appearance of polarization as shown in a single dislocation (Fig. 2 in the main text), compression may contribute to enhancing polarization in a vertical direction. For example, compression in the x_1 direction enhances polarization in x_2 direction while tension in the x_1 direction reduces polarization in x_2 direction. On the other hand, around dipole B in the dislocation wall, ferroelectric nano-region expands in the x_2 direction due to electric fields (Fig. S4(d2)). Therefore, compression in x_1 direction between dipole B does not hinder the expanding of ferroelectric nano-region or rather be favorable for expanding. And dipole A is contrary to dipole B, that is, tension in x_1 direction between dipole A may hinder the ferroelectric connection. We think that, due to these mechanisms, connectivity of dipole B gets stronger than dipole A in the dislocation wall.

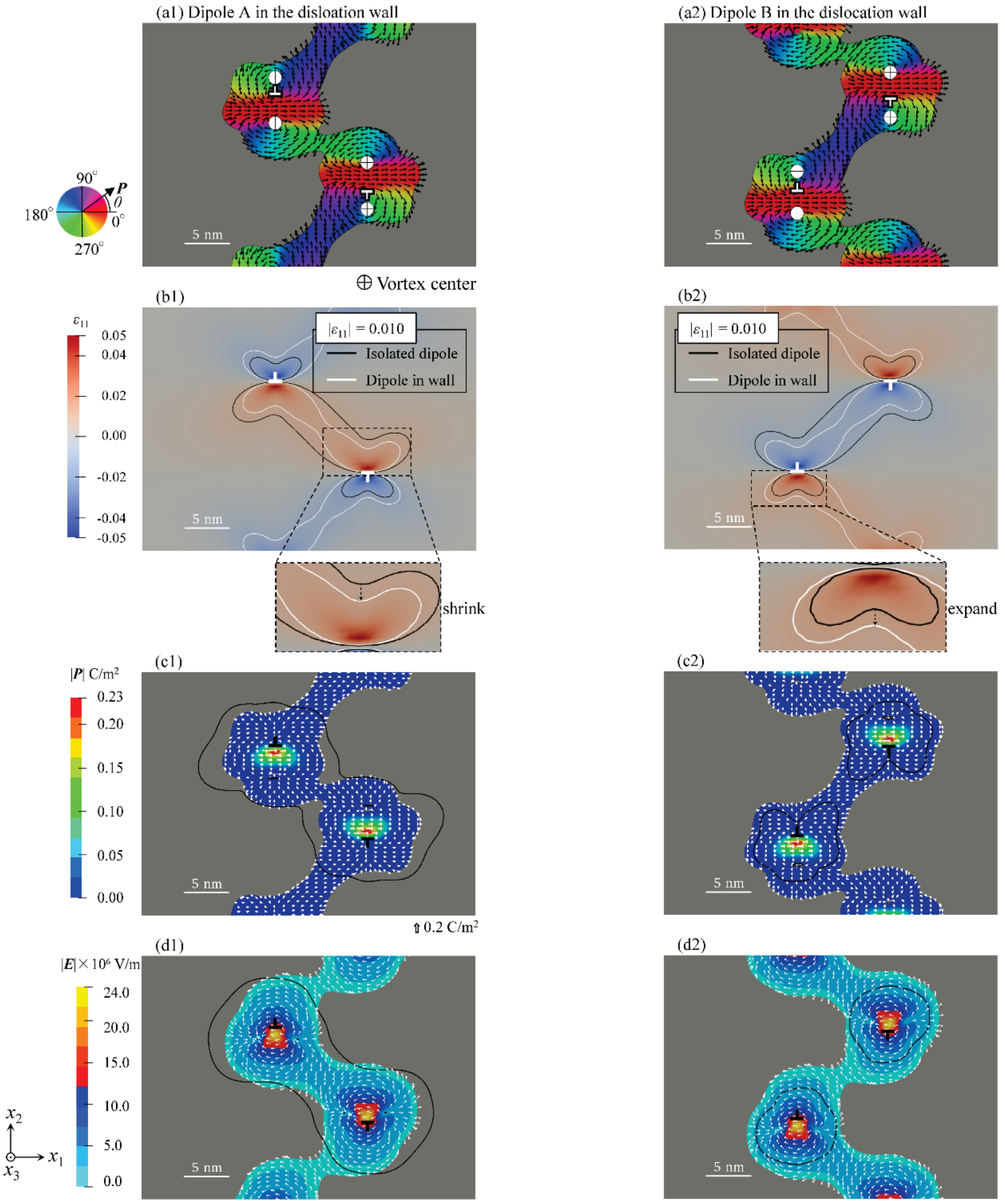

Figure S4 Polarization distributions, elastic strains, polarization magnitudes and electric fields around (a1-d1) the dipole A in the dislocation wall and (a2-d2) the dipole B in the dislocation wall. Black solid lines are corresponding physical fields of an isolated dipoles A in (a1-d1), and isolated dipole B in (a2-d2).

Reference

1 H. Uwe and T. Sakudo, *Phys. Rev. B*, 1976, **13**, 271–286.

2 J. H. Haeni, P. Irvin, W. Chang, R. Uecker, P. Reiche, Y. L. Li, S. Choudhury, W. Tian, M. E. Hawley, B. Craigo, A. K. Tagantsev, X. Q. Pan, S. K. Streiffer, L. Q. Chen, S. W. Kirchoefer, J. Levy and D. G. Schlom, *Nature*, 2004, **430**, 758–761.

3 A. Vasudevarao, A. Kumar, L. Tian, J. H. Haeni, Y. L. Li, C. J. Eklund, Q. X. Jia, R. Uecker, P. Reiche, K. M. Rabe, L. Q. Chen, D. G. Schlom and V. Gopalan, *Phys. Rev. Lett.*, 2006, **97**, 257602.

4 H. Unoki and T. Sakudo, *J. Phys. Soc. Jpn.*, 1967, **23**, 546–552.

5 U. Aschauer and N. A. Spaldin, *J. Phys. Condens. Matter*, 2014, **26**, 122203.

6 G. Sheng, Y. L. Li, J. X. Zhang, S. Choudhury, Q. X. Jia, V. Gopalan, D. G. Schlom, Z. K. Liu and L. Q. Chen, *J. Appl. Phys.*, 2010, **108**, 084113.

7 G. Sheng, Y. L. Li, J. X. Zhang, S. Choudhury, Q. X. Jia, V. Gopalan, D. G. Schlom, Z. K. Liu and L. Q. Chen, *Appl. Phys. Lett.*, 2010, **96**, 232902.

8 Y. L. Li, S. Choudhury, J. H. Haeni, M. D. Biegalski, A. Vasudevarao, A. Sharan, H. Z. Ma, J. Levy, V. Gopalan, S. Trolier-McKinstry, D. G. Schlom, Q. X. Jia and L. Q. Chen, *Phys. Rev. B*, 2006, **73**, 184112.

9 S. Y. Hu and L. Q. Chen, *Acta Mater.*, 2001, **49**, 463–472.

10 S. Y. Hu and L. Q. Chen, *Acta Mater.*, 2004, **52**, 3069–3074.

11 B. K. Choudhury, K. V. Rao and R. N. P. Choudhury, *J. Mater. Sci.*, 1989, **24**, 3469–3474.

12 J. P. Hirth and J. Lothe, *Theory of Dislocations*, Krieger Publishing Company, Malabar, Fl, 1982.

13 H. H. Wu, J. Wang, S. G. Cao, L. Q. Chen and T. Y. Zhang, *J. Appl. Phys.*, 2013, **114**, 164108.

14 J. J. Wang, X. Q. Ma, Q. Li, J. Britson and L. Q. Chen, *Acta Mater.*, 2013, **61**, 7591–7603.

15 J. J. Wang, Y. Song, X. Q. Ma, L. Q. Chen and C. W. Nan, *J. Appl. Phys.*, 2015, **117**, 043907.

16 P. Yu, S. Y. Hu, L. Q. Chen and Q. Du, *J. Comput. Phys.*, 2005, **208**, 34–50.

17 P. Song, T. Yang, Y. Ji, Z. Wang, Z. Yang, L. Q. Chen and L. Chen, *Commun. Comput. Phys.*, 2017, **21**, 1325–1349.

18 L. Q. Chen and J. Shen, *Comput. Phys. Commun.*, 1998, **108**, 147–158.

19 H. L. Hu and L. Q. Chen, *J. Am. Ceram. Soc.*, 1998, **81**, 492–500.